Electronic Supplementary Material (ESI) for Nanoscale Advances.

Mapping Complex Profiles of Light Intensity with Interferometric Lithography

Supplementary Information

Joseph Holmes,[†] Mi Zhang,[‡] Tine Greibe,[‡] William L. Schaich,[†] Stephen C. Jacobson,[*,‡] and Bogdan Dragnea[*,‡]

[†]*Physics Department, Indiana University, Bloomington, IN 47405, U.S.*

[‡]*Department of Chemistry, Indiana University, Bloomington, IN 47405, U.S.*

E-mail: jacobson@iu.edu; dragnea@iu.edu

Phone: +1 (812) 8560087

Averages

To compute the local electric field intensity, we start with an incident plane wave at frequency ω moving from the glass along the z-axis (normal to the metal plane) and polarized along $\hat{x}$:

$$\vec{\mathrm{E}}^{(1)}_{\mathrm{inc}}(\vec{\mathbf{r}},t) = \mathrm{Re}\{\hat{x}\mathrm{E}_0 e^{i(\mathrm{k_g}z-\omega t)}\}, \tag{1}$$

where $\mathrm{k_g} = \mathrm{n_g}\omega/\mathrm{c}$ and Re{...} denotes the real part of {...}. From this information, plus the geometry and refraction indices of the glass, metal, and polymer media, the FDTD solver computes a total field, linearly proportional to E_0, described by:

$$\vec{\mathrm{E}}^{(1)}_{\mathrm{tot}}(\vec{\mathbf{r}},t) = \mathrm{Re}\{\vec{\mathrm{E}}^{(1)}_{\mathrm{tot}}(\vec{\mathbf{r}},\omega)e^{-i\omega t}\}\ . \tag{2}$$

The structures in the experiments are produced by the time-averaged (over the light period $2\pi/\omega$) square of the total field[1]

$$\langle\left|\vec{\mathrm{E}}^{(1)}_{\mathrm{tot}}(\vec{\mathbf{r}},t)\right|^2\rangle = \frac{1}{2}\left|\vec{\mathrm{E}}^{(1)}_{\mathrm{tot}}(\vec{\mathbf{r}},\omega)\right|^2\ . \tag{3}$$

To account for an unpolarized incident beam, we have the software do a separate calculation for an incident wave with the same amplitude and frequency but polarized along $\hat{y}$:

$$\vec{\mathrm{E}}^{(2)}_{\mathrm{inc}}(\vec{\mathbf{r}},t) = \mathrm{Re}\{\hat{y}\mathrm{E}_0 e^{i(\mathrm{k_g}z-\omega t)}\}, \tag{4}$$

If we combine these two incident fields via

$$\vec{\mathrm{E}}_{\mathrm{inc}}(\vec{\mathbf{r}},t) = \vec{\mathrm{E}}^{(1)}_{\mathrm{inc}}(\vec{\mathbf{r}},t)\cos(\phi) + \vec{\mathrm{E}}^{(2)}_{\mathrm{inc}}(\vec{\mathbf{r}},t)\sin(\phi)\ , \tag{5}$$

the angle ϕ describes a linear polarization angle with respect to the x-axis. This $\vec{\mathrm{E}}_{\mathrm{inc}}$ formally leads to

$$\vec{\mathrm{E}}_{\mathrm{tot}}(\vec{\mathbf{r}},t) = \vec{\mathrm{E}}^{(1)}_{\mathrm{tot}}(\vec{\mathbf{r}},t)\cos(\phi) + \vec{\mathrm{E}}^{(2)}_{\mathrm{tot}}(\vec{\mathbf{r}},t)\sin(\phi)\ , \tag{6}$$

so the corresponding time and polarization average of $\left|\vec{\mathrm{E}}_{\mathrm{tot}}\right|^2$ is

$$\langle\langle\left|\vec{\mathrm{E}}_{\mathrm{tot}}(\vec{\mathbf{r}},t)\right|^2\rangle\rangle = \frac{1}{4}\sum_{\alpha=1}^{2}\left|\vec{\mathrm{E}}_{\mathrm{tot}}^{(\alpha)}(\vec{\mathbf{r}},\omega)\right|^2 . \tag{7}$$

Relative permittivities

By working in the time domain to produce an $\vec{\mathrm{E}}_{\mathrm{tot}}(\vec{\mathbf{r}},t)$ the effect of the permittivity formally enters through a convolution integral for the displacement field

$$\vec{\mathrm{D}}_{\mathrm{tot}}(\vec{\mathbf{r}},t) = \int_{-\infty}^{t} dt'\epsilon(\vec{\mathbf{r}},t-t')\vec{\mathrm{E}}_{\mathrm{tot}}(\vec{\mathbf{r}},t') \tag{8}$$

The FDTD software starts for the metal with permittivity values at discrete frequencies.[2] It then interpolates this data set and, using an inverse Fourier transform, determines $\varepsilon(t-t')$. In Fig.S1 we plot the interpolated, complex-valued relative permittivity for Cr and Al. There is a considerable difference between the two metals.

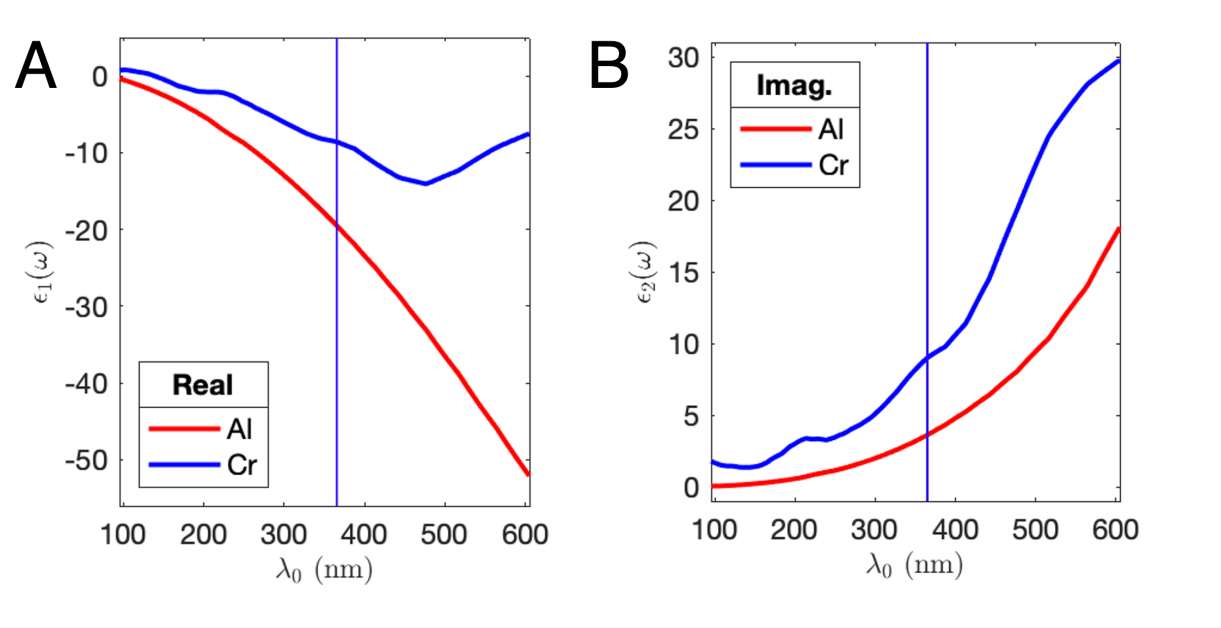

Figure S1: Complex, frequency-dependent relative permittivities of two real metals Al (red) and Cr (blue). The real part (A) and imaginary (B) are plotted for each metal separately. The vertical line is at $\lambda_0 = 365$ nm.

Waveguide propagation

To develop understanding of and confidence in the numerical calculations, we have examined several simplified models where analytic results can be obtained. Consider for instance how light moves within a single hole. Viewing the hole channel as a circular waveguide, we ask what propagation modes are possible. Switching to cylindrical, polar coordinates (ρ, ϕ, z) and assuming the metal is a perfect conductor, an appropriate form of the axial magnetic field inside the guide (a TE mode) is

$$\mathrm{B_z} \propto \mathrm{J_1}(\gamma_\mathrm{p}\rho)\sin(\phi)\mathrm{e}^{\mathrm{ik_z z}} \,, \tag{9}$$

where $\gamma_\mathrm{p}^2 = \left(\frac{\omega}{\mathrm{c}}\right)^2 \varepsilon_\mathrm{p} - \mathrm{k}_z^2 \,, \varepsilon_\mathrm{p} = \mathrm{n}_\mathrm{p}^2$, and $\mathrm{J_1}$ is a Bessel function.[1] The angular dependence here is consistent with the incident light being (electric) polarized along $\phi = 0$. The transverse components of $\vec{\mathrm{B}}$ and $\vec{\mathrm{E}}$ are determined by derivatives of $\mathrm{B_z}$, while $\mathrm{E_z} = 0$. The mode's propagation wavevector, k_z, is determined by the boundary condition around the guide wall, $\rho = \mathrm{r}$, of[1]

$$\frac{\mathrm{dJ_1}(\gamma_\mathrm{p}\rho)}{\mathrm{d}\rho}|_{\rho=r} = 0 \tag{10}$$

Since the first zero of $\mathrm{dJ_1}(\nu)/\mathrm{d}\nu$ is at $\nu = 1.841$, the $\mathrm{TE_{11}}$ mode dispersion becomes

$$\mathrm{k_z^2} = \left(\frac{\omega}{\mathrm{c}}\right)^2 \varepsilon_\mathrm{p} - \left(\frac{1.841}{\mathrm{r}}\right)^2 = \left(\frac{2\pi \mathrm{n_p}}{\lambda}\right)^2 - \left(\frac{1.841}{\mathrm{r}}\right)^2 \,. \tag{11}$$

In order for this mode to propagate, one needs $\mathrm{k}_z^2 > 0$. The vacuum wavelength at cutoff is thus set by $\mathrm{k}_z^2 = 0$ so

$$\lambda_\mathrm{c} = 2\pi \mathrm{r n_p}/1.841 = 287 \text{ nm} \tag{12}$$

for our holes of radius $r = 50$ nm filled with polymer of $\mathrm{n_p} = 1.68$. Hence for a vacuum wavelength of 365 nm, this mode will exponentially decay in z:

$$e^{i\mathrm{k}_z z} -> e^{-\kappa_z z} \qquad \text{with} \qquad \kappa_z = 1/43.9 \text{ nm}. \tag{13}$$

Other zeros of $dJ_1(\nu)/d\nu$ lead to even smaller wavelength cutoffs and more rapid decay. If we switch to TH modes the axial field is then electric

$$E_z \propto J_1(\gamma_p \rho)\cos(\phi)e^{ik_z z} \tag{14}$$

with $B_z = 0$ and transverse components of $\vec{E}$ and $\vec{B}$ determined by derivatives of E_z plus the new boundary condition of $J_1(\gamma_p r) = 0$, which first occurs at $\gamma_p r = 3.832$.[1] This leads to a vacuum wavelength at cutoff for the TM_{11} mode of

$$\lambda_c = \frac{2\pi r n_p}{3.832} = 138 \text{ nm}. \tag{15}$$

All of these estimates imply that for a metal thickness of 100 nm the time-averaged square of the associated fields will decay by two (or more) orders of magnitude in moving through the hole, while the FDTD calculations show a decay by less than a factor of five.

So we next consider the metal to be less than perfect, which allows the fields to penetrate into the metal. This extension means Eq. 9 and Eq. 14 have to be supplemented with terms in $\rho > r$. Since ε_m has a large negative real part, the γ_m^2 does too, so we replace it with $\alpha_m^2 = -\gamma_m^2$ and for $\rho > r$ the J_1 in Equations 9 and 14 with $K_1(\alpha_m \rho)$, where K_1 is a modified Bessel function. The new boundary conditions across $\rho = r$ cannot be satisfied by a TE or TM mode alone. One needs to form a linear combination of the two which leads to a complicated transcendental equation to be solved for $k_z(\omega)$.[3,4] The solution of this equation is considerably simplified if one uses a Drude model without dissipation for the metal's dielectric function

$$\varepsilon_m^D = 1 - \left(\frac{\omega_p^2}{\omega^2}\right) , \tag{16}$$

with ω_p the plasma frequency.[5,6] The key approximation is that the ε_m^D has no imaginary part, so compared to the physical metal's dielectric function, $\varepsilon_m = n_m^2$, it is more reasonable for Al than Cr - see Figure S1. Consequently we focus our discussion on Al. For Al we use

$\hbar\omega = 15.6$ eV and seek solutions that have a real valued k_z. Instead of a single cutoff, there are passbands that have $k_z^2 > 0$.[6] The lowest energy passband for r = 50 nm and $n_p = 1.68$ lies between vacuum wavelengths of 400 nm to 156 nm. Hence our case of $\lambda_0 = 365$ nm is just below the long wavelength cutoff of this passband. We checked that modest changes in the system's parameters can push one past the cutoff. For instance using $r = 40$ nm or replacing $n_p \to n_g = 1.47$ leads to $k_z^2 < 0$ when $\lambda_0 = 365$ nm.

To check how much the retention of the imaginary part in ε_m matters, we also solved the full transcendental equation for k_z when $\lambda_0 = 365$ nm. We write the answer as $k_z = 2\pi/p + i/\delta$, where p is a period and δ a decay length. Table 1 summarizes the results. The

Table 1

	p(nm)	$\delta(nm)$
Al (ε_m^D)	494	–
Al (ε_m)	473	511
Cr (ε_m)	356	134

effect of dissipation in Al is modest: the period is hardly changed and the decay length is much greater than our metal thickness.[7] We have also included the result for Cr, which has a smaller δ, as expected.

Once k_z is known all field components can be analytically calculated, to within a common scale factor. Comparing these profiles at fixed z with the corresponding ones produced by FDTD at z midway through the hole channel, we found reasonable agreement. For both Al and Cr the relative strength of $|B_z|$ is greater (in cgs units) than that of $|E_z|$, which means the mode may be labeled as HE_{11}. At the high energy (short wavelength) limit of the lowest passband, $k_z \to \infty$, and the cutoff frequency is set by $\varepsilon_m^D(\omega) + \varepsilon_p = 0$.[6,8] This result is satisfied by the electrostatic surface plasmon frequency for a flat surface between the metal and polymer. The mode has a purely TM symmetry so its waveguide label has become EH_{11}.

The weak decay of the HE_{11} mode moving through a hole in a real (as opposed to

a perfectly conducting) metal suggests that Fabry Pérot effects should occur when back scattering from the exit and entrance regions is included.[9,10] The evidence for standing waves is not clear for our metal thickness of $h = 100$ nm because of end effects where fields are enhanced around the hole's rim. However when h is increased into the range $400 - 600$ nm, the spatial decay of $\langle\langle \left|\vec{\mathrm{E}}_{\mathrm{tot}}(\vec{\mathbf{r}}, t)\right|^2 \rangle\rangle$, Eq. 7 , away from the ends shows nonmonotonic decay with local peaks separated by ≈ 250 nm in Al, consistent with the results in Table 1.

Isosurface intensity values

Rather than repeatedly creating several intensity isosurfaces and looking for the best match with the measured replicas in Figures 4-6, it is enough to do this matching process for just one case. The equation defining the threshold isointensity surface, $I(\vec{\mathbf{r}})$, for a so-called case 1 is

$$\Phi_{th} = \tau_1 I_1(\vec{\mathbf{r}}_1) \tag{17}$$

where the specific $\vec{\mathbf{r}}_1$ can be taken as the location of the highest point on the intensity isosurface that best matches with the the highest point on the replica for case 1. Next consider a case 2 with the same pulse duration. The analog of Eq.17 is

$$\Phi_{th} = \tau_1 I_2(\vec{\mathbf{r}}_2) \tag{18}$$

where $\vec{\mathbf{r}}_2$ is at the highest point on the case 2 intensity isosurface. Comparing these two equations we deduce that

$$I_2(\vec{\mathbf{r}}_2) = I_1(\vec{\mathbf{r}}_1) \tag{19}$$

which means that the intensity on the case 2, threshold intensity isosurface is identical to that on the case 1 isosurface. For Figures 4,5,6 the pulse duration is the same in every case, so the threshold isosurface intensity values must all be the same, independent of the number or arrangement of apertures.

However for Figure 3 the pulse duration was doubled for a case 3 with $\tau_3 = 2\tau_1$, which implies that

$$I_3(\vec{\mathbf{r}}_3) = I_1(\vec{\mathbf{r}}_1)/2 \tag{20}$$

This reduction of intensity on the case 3, threshold intensity isosurface was confirmed by visual matching in Figure 3.

References

(1) Jackson, J. D. *Classical Electrodynamics*, 3rd ed.; Wiley, 1999.

(2) Palik, E. D. *Handbook of Optical Constants of Solids*; Academic Press: Boston, 1998.

(3) Stratton, J. A. *Electromagnetic Theory*; John Wiley & Sons, Ltd, 2015.

(4) Tsang, L.; Kong, J. A.; Ding, K.-H. *Scattering of Electromagnetic Waves: Theories and Applications*; John Wiley & Sons, Ltd, 2000.

(5) Pfeiffer, C. A.; Economou, E. N.; Ngai, K. L. Surface polaritons in a circularly cylindrical interface: Surface plasmons. *Phys. Rev. B* **1974**, *10*, 3038–3051.

(6) Shin, H.; Catrysse, P. B.; Fan, S. Effect of the plasmonic dispersion relation on the transmission properties of subwavelength cylindrical holes. *Phys. Rev. B* **2005**, *72*, 085436.

(7) Webb, K. J.; Li, J. Analysis of transmission through small apertures in conducting films. *Phys. Rev. B* **2006**, *73*, 033401.

(8) Xu, H.; Zhu, P.; Craighead, H. G.; Webb, W. W. Resonantly enhanced transmission of light through subwavelength apertures with dielectric filling. *Optics Communications* **2009**, *282*, 1467–1471.

(9) Olkkonen, J.; Kataja, K.; Howe, D. G. Light transmission through a high index dielectric-filled sub-wavelength hole in a metal film. *Opt. Express* **2005**, *13*, 6980–6989.

(10) Bai, M.; García, N. Transmission of light by a single subwavelength cylindrical hole in metallic films. *Applied Physics Letters* **2006**, *89*, 141110.